Original Article

Highly Pluripotent Adipose-Derived Stem Cell–Enriched Nanofat: A Novel Translational System in Stem Cell Therapy

Cell Transplantation
Volume 32: 1–16

DOI: 10.1177/09636897231175968
journals.sagepub.com/home/cll
Sage

Lindsey Alejandra Quintero Sierra[1*], Reetuparna Biswas[1*], Anita Conti[1*], Alice Busato[1,2], Riccardo Ossanna[1], Nicola Zingaretti[3], Pier Camillo Parodi[3,4], Giamaica Conti[1], Michele Riccio[4,5†], Andrea Sbarbati[1,4], and Francesco De Francesco[5†]

Abstract

Fat graft is widely used in plastic and reconstructive surgery. The size of the injectable product, the unpredictable fat resorption rates, and subsequent adverse effects make it tricky to inject untreated fat into the dermal layer. Mechanical emulsification of fat tissue, which Tonnard introduced, solves these problems, and the product obtained was called nanofat. Nanofat is widely used in clinical and aesthetic settings to treat facial compartments, hypertrophic and atrophic scars, wrinkle attenuation, skin rejuvenation, and alopecia. Several studies demonstrate that the tissue regeneration effects of nanofat are attributable to its rich content of adipose-derived stem cells. This study aimed to characterize *Hy-Tissue Nanofat* product by investigating morphology, cellular yield, adipose-derived stem cell (ASC) proliferation rate and clonogenic capability, immunophenotyping, and differential potential. The percentage of SEEA3 and CD105 expression was also analyzed to establish the presence of multilineage-differentiating stress-enduring (MUSE) cell. Our results showed that the *Hy-Tissue Nanofat* kit could isolate $3.74 \times 10^4 \pm 1.31 \times 10^4$ proliferative nucleated cells for milliliter of the treated fat. Nanofat-derived ASC can grow in colonies and show high differentiation capacity into adipocytes, osteocytes, and chondrocytes. Moreover, immunophenotyping analysis revealed the expression of MUSE cell antigen, making this nanofat enriched of pluripotent stem cell, increasing its potential in regenerative medicine. The unique characteristics of MUSE cells give a simple, feasible strategy for treating a variety of diseases.

Keywords

nanofat, stromal vascular fraction, adipose stem cells, stem cell therapy, mechanical disaggregation, translational therapy

Introduction

The autologous fat graft is used mainly in aesthetic medicine, particularly for face rejuvenation and volume restoration, and also for reconstructive purposes such as breast reconstruction, hypertrophic scars, and painful hand neuromas, thanks to its simple harvesting through liposuction and its autogenous and biocompatible nature[1]. Nevertheless, fat graft presents some limitations, such as the size of the injectable product, the unpredictable fat resorption rates[2], and subsequent adverse

[1] Human Anatomy and Histology Section, Department of Neuroscience, Biomedicine, and Movement, University of Verona, Verona, Italy
[2] Safety Assessment Department, Aptuit (Verona) S.r.l., an Evotec Company, Verona, Italy
[3] Department of Medical Area (DAME), Clinic of Plastic and Reconstructive Surgery, Academic Hospital of Udine, University of Udine, Udine, Italy
[4] Research and Training Center in Regenerative Surgery, Accademia del Lipofilling, Montelabbate, Italy
[5] Department of General and Specialties Surgery, SOD of Reconstructive Surgery and Hand Surgery, Azienda Ospedaliera Universitaria delle Marche, Ancona, Italy

*The authors contributed equally to the work
†Equally corresponding authors.

Submitted: November 23, 2022. Revised: April 25, 2023. Accepted: April 29, 2023.

Corresponding Authors:
Francesco De Francesco, Department of General and Specialties Surgery, SOD of Reconstructive Surgery and Hand Surgery, Azienda Ospedaliera Universitaria delle Marche, Via Conca 71, 60126 Ancona, Italy.
Email: francesco.defrancesco@ospedaliriuniti.marche.it

Michele Riccio, Department of General and Specialties Surgery, SOD of Reconstructive Surgery and Hand Surgery, Azienda Ospedaliera Universitaria delle Marche, Via Conca 71, 60126 Ancona, Italy.
Email: michele.riccio@ospedaliriuniti.marche.it

events[3]. Moreover, injecting the fat graft into the dermal layer to treat superficial rhytides, wrinkles, and atrophic scars is still challenging[4]. Therefore, many patients still need to be convinced to use this procedure. Fortunately, modern commercial medical devices are able to make up for the shortcomings of the original techniques[5].

Moreover, during the last years, surgeons and researchers tested different protocols to manipulate fat and inject it rapidly without inflammatory reactions. In particular, the adipose tissue should be able to integrate within the damaged tissue through sufficient vascularization adequately. This makes the fate of the fat uncertain when used as a volumetric filler. Derivatives of adipose tissue, such as microfat, nanofat, microvascular fragments, stromal vascular fraction, and stem cells, are not only commonly used in research but also clinically to enhance the vascularization of implants and grafts at defect sites. In plastic surgery, adipose tissue is harvested via liposuction and can be manipulated in three ways (macrofat, microfat, and nanofat) in the operating room, depending on its ultimate use and on the disgregation system[6]. Whereas macrofat and microfat are used as a filling material, nanofat is a viscous extract that can induce tissue remodeling because it is rich in growth factors and stem cells[6].

Nanofat is defined as an autologous liquid-like tissue obtained through the mechanical manipulation of lipoaspirates. During the process, the harvested fat is filtered and shuffled between two 10-ml syringes with a 30 passes connector, destroying nearly all adipocytes, resulting in a purified emulsion product[6]. The final product can be directly injected into the target site with high precision, even in difficult areas, allowing it to work superficially with still finer sharp needles (27 or 30 gauge)[7,8]. Nanofat is widely used in clinical practice to treat facial compartments, hypertrophic and atrophic scars, wrinkle attenuation, skin rejuvenation, and alopecia[9–12]. Recently, nanofat has been investigated for broader applications, such as wound healing by the paracrine effect of nanofat product[1,13]. The regenerative effect of nanofat is attributable to the presence of microfragments of stromal connective tissue composed of adipose-derived stem cells (ASCs), endothelial precursor cells, endothelial cells, macrophages, smooth muscle cells, lymphocytes, pericytes, and pre-adipocytes[1,14–16]. The nanofat main secretome consists of proliferative, pro-angiogenic, pro-differentiative, and pro-antiapoptotic factors such as platelet-derived growth factor (PDGF), vascular endothelial growth factor (VEGF), and insulin-like growth factor (IGF), among others[14,17].

Among the cellular components of nanofat, ASCs represent the leading actor of tissue regeneration, cooperating with other cellular elements in the process of restitutio ad integrum[18]. ASCs are adult plastic-adherent mesenchymal stem cells easily isolable from adipose tissue, allowing autologous cell transplantation[19,20]. According to the literature, ASCs module the inadequate healing responses, which lead to tissue degeneration such as chronic inflammation[21], hypermetabolic responses[22], and fibrosis[23]. Moreover, ASCs stimulate extracellular matrix production, new collagen deposition, and early revascularization[24,25]. Initial *in vitro* experiments demonstrated the angiogenic effect of ASC[26], which was then attributed to the presence of the secretome[27]. Their biological effect is due to the self-renewal property, immunosuppressive potential, and ability to differentiate into different mesodermal cell lineages, such as adipocytes, osteocytes, and chondrocytes[28–30]. For these reasons, *in vitro* characterization of nanofat in terms of ASCs content could reflect the regenerative potential of the product, indicating how many cells are capable of duplicating and differentiating in a short period of time, which can guarantee a replicable result for patients and reduce the recovery time.

Recent studies have focused on a subpopulation of mesenchymal stem cells defined as multilineage-differentiating stress-enduring (MUSE) cells. MUSE cells are defined as non-tumorigenic stress-tolerant and pluripotent cells with high regenerative potential[31–34] and migration capacity into the damaged tissue[35]. MUSE cells were isolated from different sources such as skin, bone marrow, and hair bulbs, but principally were isolated from adipose tissue, in which researchers found a higher number of MUSE cells[36–38]. MUSE cells are characterized by high integration capacity and restoration of tissue function, as evidenced in numerous preclinical studies[34,39]. Thanks to their unique features, MUSE cells are a promising candidate for tissue regeneration and stem cell therapy.

This study aimed to characterize at the morphological and cellular level a promising and standardized single-use assembled system named *Hy-Tissue Nanofat* that allows obtaining a final product enriched in pluripotent and proliferative ASCs with highly potential use in clinical practice.

Materials and Methods

Adipose Tissue Collection

The adipose tissue was collected from eight women undergoing liposuction for aesthetic purposes, aged between 41 and 69 years. Informed consent was taken before collecting lipoaspirates following the ethical guidelines established by the review committee for human studies of AOU "Ospedali Riuniti," Ancona, Italy (Micro-adipose graft_01, 18 May 2017). Klein solution (2% lidocaine solution: 0.08% w/v; adrenaline 1 mg/ml solution: 0.1% v/v in 0.9% saline) was injected 10 min after the liposuction. A cannula of 11 G, 6 holes, and a 20-ml Vac-Lock syringe provided with the Hy-Tissue Nanotaf Plus system was used to obtain lipoaspirate (about 30 ml of fat from each donor) from the abdominal area. The fat was transported in an adiabatic container to the laboratory and processed within 20 h from harvest.

Procedure for Nanofat-Derived Microfragment Production

Each adipose tissue sample (about 30 ml) was divided into three portions. The first portion (about 10 ml) was processed with the *Hy-Tissue Nanofat* system (Fidia Farmaceutici, Abano Terme, Italy). The lipoaspirate was shuffled and emulsified through two 10 ml coupled syringes via a 30 passes connector. The emulsified lipoaspirate was filtered into the inner bag with a pore size of 120 μm and was collected into a lower syringe.

To characterize the product at a cellular level, it was centrifuged at 3,000 × *g* for 6 min and filtered through a 70-μm nylon mesh. The product obtained by this method was named "Nanofat-derived SVF (N-ASC)."

Enzymatic Digestion of Fat

The second portion of lipoaspirate (about 10 ml) was processed using an enzymatic method, as reported by Busato et al.[30] The samples were digested with collagenase type I at a concentration of 1 mg/ml (GIBCO Life Technologies, Monza, Italy) dissolved in Hank's Balanced Salt Solution (HBSS; GIBCO Life Technologies) with 2% of bovine serum albumin (BSA; GIBCO Life Technologies) for 45 min at 37°C. Complete culture medium [Dulbecco's Modified Eagle Medium (DMEM); Sigma-Aldrich, Milan, Italy], supplemented with 10% of fetal bovine serum (FBS; GIBCO Life Technologies), 1% of 1:1 penicillin/streptomycin (P/S solution; GIBCO Life Technologies), and 0.6% of amphotericin B (GIBCO Life Technologies), was added to neutralize the enzyme action. After the neutralization process, the sample was centrifuged at 3,000 × *g* for 5 min. The cell pellet was incubated with 1 ml of erythrocyte lysis buffer 1× (Macs Miltenyi Biotec, Milan, Italy) for 10 min at room temperature. Again, the cell suspension was centrifuged and resuspended with 1 ml of complete culture medium. Finally, the cells were filtered through a 70-μm nylon mesh. The product obtained by this method was named "collagenase-derived ASCs (ED-ASCs)."

Enzymatic Digestion of Hy-Tissue Nanofat-SVF

The remaining portion of lipoaspirate (10 ml) was first processed with the *Hy-Tissue Nanofat kit*, followed by the treatment with collagenase type I. The Nanofat-SVF obtained, as described section "Adipose Tissue Collection," was incubated with collagenase type I at a concentration of 1 mg/ml (GIBCO Life Technologies) dissolved in HBSS (GIBCO Life Technologies) with 2% of BSA (GIBCO Life Technologies) for 45 min at 37°C. Complete culture medium (DMEM; Sigma-Aldrich), supplemented with 10% of FBS (GIBCO Life Technologies), 1% of 1:1 penicillin/streptomycin (P/S solution; GIBCO Life Technologies), and 0.6% of amphotericin B (GIBCO Life Technologies), was added to neutralize the enzyme action. After the neutralization process, the sample was centrifuged at 3,000 × *g* for 5 min. The cell pellet was incubated with 1 ml of erythrocyte lysis buffer 1× (Macs Miltenyi Biotec) for 10 min at room temperature. Again, the cell suspension was centrifuged and resuspended with 1 ml of complete culture medium. Finally, the cells were filtered through a 70-μm nylon mesh.

The product obtained by this method was named "enzymatic digestion of Nanofat-SVF (N-ED-ASCs)."

Table 1 summarizes the code names used to identify the different processes employed to treat the fat tissue.

Table 1. Code Names of the Products Obtained With the Evaluated Protocols for Fat Tissue Digestion.

Evaluated protocol	Code name
Nanofat-derived SVF	N-ASC
Collagenase-derived ASC	ED-ASC
Enzymatic digestion of Nanofat-SVF	N-ED-ASC

ASC: adipose-derived stem cell.

Morphological Analysis

To evaluate the morphology of the *Hy-Tissue Nanofat*, SVF whole-mount assay was performed, as reported in Busato et al.[30] The emulsion was swiped in a histological glass and stained with toluidine blue (Sigma-Aldrich). All slides were examined under an Olympus BX-51 microscope (Olympus, Tokyo, Japan) equipped with a digital camera (DKY-F58 CCD JVC, Yokohama, Japan). In addition, for a deeper morphological understanding, the *Hy-Tissue Nanofat*-SVF was studied in scanning electron microscopy (SEM). The sample was fixed with glutaraldehyde 2% diluted in 0.1 M phosphate buffer (pH 7.4) for 2 h at 4°C and post-fixed in 1% osmium tetroxide (OsO_4) diluted in 0.2 M potassium hexacyanoferrate for 1 h at 4°C. The samples were dehydrated in a graded concentration of ethanol, followed by a critical point dryer (CPD 030, Balzers, Vaduz, Liechtenstein), mounted to stubs with colloidal silver and sputtered with gold by an MED 010 coater (Balzers), and examined with FEI XL30 scanning electron microscope (FEI Company, Eindhoven, The Netherlands). All the morphological analyses were performed on each sample collected from every patient.

Cellular Yield

Collected cells from the evaluated procedures were counted using trypan blue exclusion assay using a CytoSMART counter (Automated Image-Based Cell Counter, version 1.5.0.16380; CytoSMART Technologies B.V, Eindhoven, The Netherlands), which indicates the number of living cells in a sample. Cell yield was calculated considering the total amount of living cells of N-ASC, ED-ASC, and N-ED-ASC divided by the fat volume.

Proliferation Capacity

To evaluate the cell proliferation capacity of the cells derived from the three different isolation procedures (N-ASC, ED-ASC, and N-ED-ASC), 2×10^5 cells of each procedure were plated on a 25-cm^2 T-flask and incubated in a humidified atmosphere with 5% CO_2 at 37°C in triplicate for each procedure. The complete culture medium was changed 72 h after the cell extraction and, subsequently, every 48 h until 80% confluence. The days required for the cultured cells to reach confluence (cellular passage 1) were used for determining the proliferation capacity. Furthermore, the population doubling time (PDT) assay was performed to estimate the time request for cell replication. Four days after the seeding, 5×10^4 cells from N-ASC, ED-ASC, and N-ED-ASC were plated in T-25 Flasks (in triplicate) with 4 ml of complete culture media. They were incubated in a humidified atmosphere with 5% CO_2 at 37°C for different time points, 24, 72, and 96 h. At each time point, after a brief wash with PBS, the cells were incubated with 0.25% trypsin (GibcoBRL/Life Technologies) at 37°C for 5 min, centrifuged, and the cell pellet was resuspended in 1 ml of complete culture media. CytoSMART counter (Automated Image-Based Cell Counter, version 1.5.0.16380; CytoSMART Technologies) was used to detect the number of cells at each time point. PDT was calculated using the following equation: $PDT = [t(h) \times \log 2]/\log (Nf/Ni)$[40], where Ni and Nf are initial and final cell numbers, respectively.

Clonogenic Capacity

N-ASC, ED-ASC, and N-ED-ASC were seeded in a six-well plate in triplicate.

In all, 5×10^3 cells from N-ASC were plated, while 1×10^3 cells from N-ED-ASC and ED-ASC were used. Cells were cultured for 14 days. Toluidine blue (Sigma-Aldrich) staining was performed to count the colonies. The frequency of colony-forming unit-fibroblast (CFU-F) within N-ASC, ED-ASC, and N-ED-ASC was expressed as a percentage of seeded cells.

Immunophenotyping

N-ASC, ED-ASC, and N-ED-ASC and the subsequent subculture cells (cellular passage 2) were characterized by flow cytometry in triplicate. To perform cytofluorimetric analysis, the different cells product was centrifuged at 3000 $\times$ *g* for 6 min. The cell pellet obtained was resuspended in a complete culture medium, incubated with 1 ml of erythrocyte lysis buffer 1× (Macs Miltenyi Biotec, Milan, Italy) for 10 min at room temperature, and filtered through a 70-µm cell strainer. Subsequently, cells were washed with 1 ml of PBS and incubated (1×10^5 for each tube) with conjugated antibodies on ice for 30 min. After incubation, the pellets were centrifuged (5,000 rpm, 7 min) and resuspended in 100 µl of PBS.

The antibodies used were selected considering the minimal criteria to identify mesenchymal stem cells defined by the International Society of Cellular Therapies[41], which are as follows: CD105 APC conjugate (1:20 dilution), CD73 BV421 conjugate (1:20 dilution), CD34 PE conjugate (1:5 dilution), CD45 FITC conjugate (1:20 dilution), CD146 APC conjugate (1:20 dilution), and SEEA3 FITC conjugate (1:20 dilution). All antibodies were purchased from BD Biosciences (Becton Dickinson Italy S.P.A., Milano, Italy). Also, the isotypes of each antibody were incubated with cells to determine the threshold of fluorescence and to exclude no specific signal. Isotypes were indicated by the datasheet of each primary antibody and incubated with cells at the same concentration of primary antibodies.

Immunophenotyping was performed through a chant II FACS (BD, Becton Dickinson).

Differentiation Assay

The differentiation potential was evaluated *in vitro* for the N-ASC compared with ED-ASC and N-ED-ASC. Non-induced cells were used as control (CTR). Differentiation was carried out employing expanded cultured cells from passage 4. At each time point, the samples were seeded in triplicate for every differentiation protocol.

For adipogenic differentiation, 5,000 cells were seeded on a 12-well plate containing one slide per well to make the cells grow adherent and incubated at 37°C, 5% CO_2, and after 24 h; the complete culture medium was replaced with adipogenic media (Sigma-Aldrich). To evaluate the adipogenic differentiation capacity, after 4 and 9 days of incubation, the cells were fixed with Baker's fixative (Bio-Optica, Milan, Italy) for 10 min at 4°C, washed with tap water for 10 min, and stained with Oil-Red-Oil solution (Bio-Optica) for 10 min, which is the particular staining for adipocytes[42], and Mayer's hematoxylin (Bio-Optica) for 5 min. Finally, the glass coverslips were mounted with Mount Quick aqueous (Bio-Optica).

For chondrogenic differentiation, 1×10^6 cells resuspended in 5 µl of complete culture media were seeded in a 12-well plate, and after 2 h, the chondrogenic media was added (StemPro Chondrogenic Differentiation Kit; GIBCO Life Technologies). After 4 and 9 days of incubation, changing the media every 3 days, cells were fixed with 4% formaldehyde (Bio-Optica) in PBS 0.05 M for 30 min at 4°C, washed twice with distilled water, and stained with Alcian blue solution (Merck KGaA, Darmstadt, Germany) for 40 min and with Nuclear Fast Red (Bio-Optica) for 20 min. Finally, after brief dehydration, the glass coverslips were mounted with Entellan (Merck KGaA).

For osteogenic differentiation, 5,000 cells were seeded on a 12-well plate with complete culture media, and after 24 h,

the media was replaced with osteogenic media (StemPro Osteogenesis Differentiation Kit; GIBCO Life Technologies). To evaluate the osteogenic differentiation capacity, after 4 and 9 days of incubation, the cells were fixed with 4% formaldehyde (Bio-Optica) in PBS 0.05 M for 30 min at 4°C, washed twice with distilled water, and incubated with Alizarin Red Solution (Merck KGaA) for 2/3 min and Mayer's hematoxylin (Bio-Optica) for 30 s. Finally, after brief dehydration, the glass coverslips were mounted with Entellan (Merck KGaA).

The stained cells were imaged using a bright-field optical microscope, Olympus BX-51 (Olympus, Tokyo, Japan) and equipped with a digital camera (DKY-F58 CCD JVC, Yokohama, Japan). Slides were gently cleaned with ethanol, then placed on the microscope slide holder, and five images for each slide were acquired using a 20× objective for quantifying the lipid droplets and a 10× objective for the quantification of calcified and collagenous matrices. The acquired images contained 8 to 12 cells to standardize the quantification.

The semi-quantitative analysis was performed using a custom-designed Image J Software plug-in (US National Institutes of Health) in blind condition, with previously treated images (binary images). In the case of adipogenic differentiation, the number of red spots (lipid droplets) on the cytoplasm of the cell was considered. For chondrogenic and osteogenic differentiation, the area covered by collagen aggregates was stained in blue and the area covered by calcification deposits was stained in red, respectively.

Immunostaining for MUSE Detection

An immunostaining assay revealed the presence of MUSE cells in nanofat-derived ASCs at cellular passage 4. N-ASCs were seeded on a glass with a diameter of 24 mm in six-well plates in triplicates with complete medium. The wells were incubated at 37°C and 5% of CO_2. After 24 h, cells were fixed with 4% buffered formalin for 1 h at 4°C in the dark, washed three times with sterile PBS 1×, and incubated with SEEA3 (FITC conjugate, 1:200 dilution) and CD105 (APC conjugate, 1:200 dilution) antibodies in the dark at 4°C for 30 min. At the end of the incubation with the antibodies, the glasses were washed with PBS, and mounting medium containing DAPI was added. The slices were imaged with an Olympus BX-51 microscope (Olympus) equipped with a digital camera (DKY-F58 CCD JVC) at 60× objective. Images were prepared using Las-X software.

Statistical Analysis

The data were reported as mean ± standard deviation (SD). Mann–Whitney tests were performed, and differences between groups were considered statistically significant when the P value was < 0.05. All statistical analyses were performed using GraphPad Prism version 8.00 for Windows, GraphPad Software (La Jolla, CA, USA).

Results

Microscopical Analysis of Hy-Tissue Nanofat-SVF

Hy-tissue Nanofat-SVF was examined at a morphological level to investigate its composition. For this purpose, lipoaspirates were processed following the protocol recommended by the manufacturer (Fig. 1A). The adipose tissue was shuffled 30 times between two connected syringes, filtered through a membrane of 120 μm, and collected with a syringe using the lower valve port of the outer bag, resulting in an autologous whitish emulsion ready to inject.

The microscopic analysis revealed that the Nanofat-SVF was mainly composed of intact lipid droplets of different sizes (Fig. 1B). The size distribution of the lipid droplets (Fig. 1C) showed that Nanofat-SVF was composed of droplets classified in four main clusters: with a diameter lower than 60 μm (42.42 ± 10.10 μm), between 60 and 100 μm (76.59 ± 11.77 μm), between 100 and200 μm (143.43 ± 33.42 μm), and over 200 μm (245.45 ± 38.07 μm). At the end of the procedure, Hy-Tissue Nanofat-SVF appears as connective tissue micro-fragments consisting of an extracellular matrix and preserved capillaries with endothelial and perivascular cells (Fig. 1C). The morphologies observed with SEM images (Fig. 1D) show the evidence of the presence of some adipocytes, elastic fibers (dotted arrow in Fig. 1D), connective tissue lamina (asterisk in Fig. 1D), and single collagen fibers (arrow in Fig. 1D). The images show that the mechanical treatment consents to a possible scaffold-like connective tissue formation.

To characterize the *Hy-Tissue Nanofat*-SVF at a cellular level, ASCs were isolated (N-ASC) and compared with ASCs enzymatically extracted (ED-ASC). Moreover, to verify the total amount and quality of the regenerative units, the *Hy-Tissue Nanofat*-SVF was subjected to enzymatic digestion (N-ED-ASC) (see the "Materials and Methods" section). Fig. 2 shows the experimental procedure followed to characterize the product in terms of cellular yield, proliferative and clonogenic capability, immunophenotyping, and multipotential capacity.

Cell Yield, Proliferation Capacity, and Clonogenic Potential of N-ASC

The N-ASC obtained by the mechanical disaggregation was analyzed in terms of cell yield, product quality, viability, proliferation capacity, and clonogenic potential considering only the living cells after the trypan blue exclusion test for cell vitality.

The number of nucleated cells (N-ASC) for milliliter of fat obtained with the *Hy-Tissue Nanofat* system was $3.74 \times 10^4 \pm 1.31 \times 10^4$ cells/ml FAT (Fig. 3A), while the number of cells extracted after enzymatic digestion of the filtered emulsion (N-ED-ASC) and after the enzymatic digestion of fat (ED-ASC) was $1.20 \times 10^5 \pm 3.90 \times 10^4$

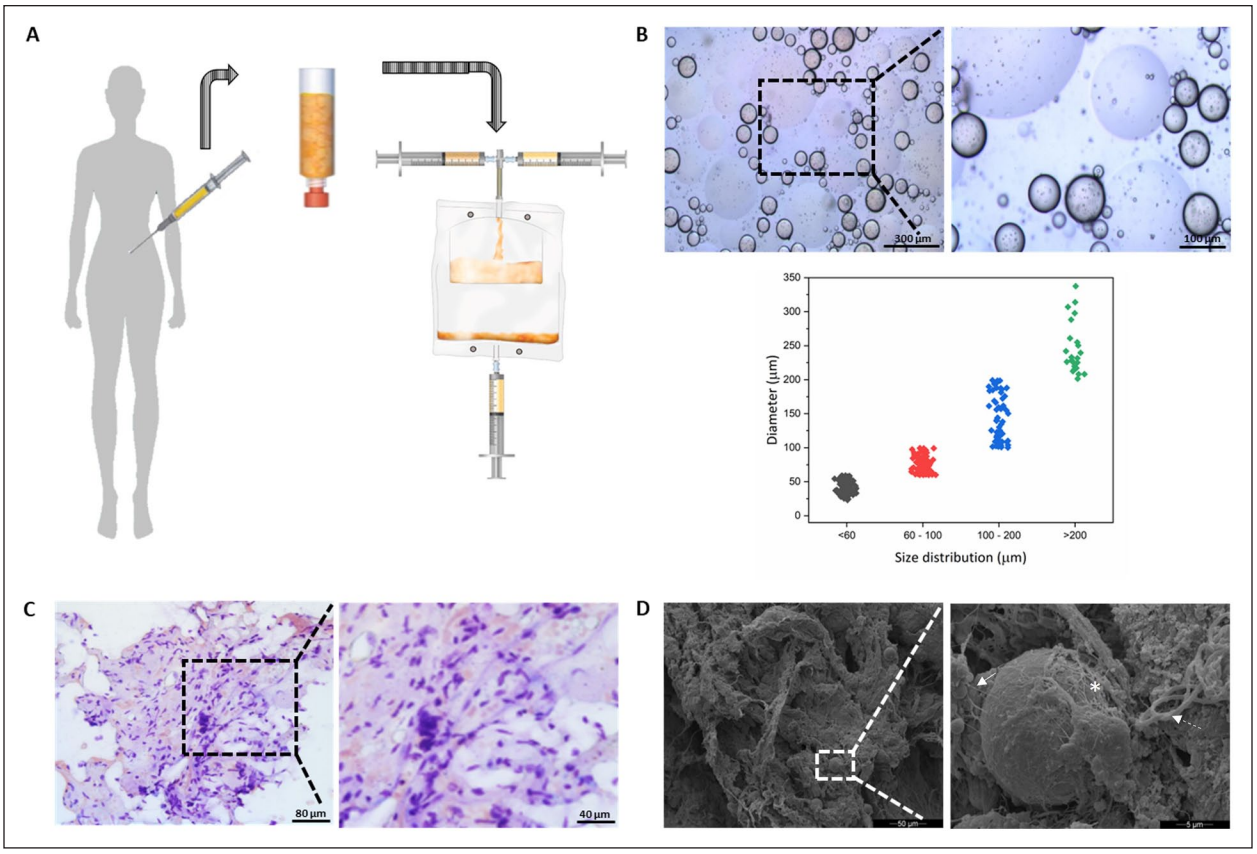

Figure 1. Morphological analysis of *Hy-Tissue Nanofat* product. Representative images were selected among the eight treated samples. (A) Scheme of the *Hy-Tissue Nanofat* procedure; (B) light microscopy of *Hy-Tissue Nanofat* product obtained with the whole-mount method. The square (in Fig. 1B, left) indicates the location of the higher magnification (right) [scale bar: (left) 300 µm, (right) 100 µm]. The graph represents the size distribution of the lipid droplets. (C). Light microscopy of *Hy-Tissue Nanofat* product obtained with the whole-mount method after centrifugation. The square (in Fig. 1C, left) indicates the location of the higher magnification (Fig. 1C, right) [scale bar: (left) 80 µm, (right) 40 µm]. (D) Scanning electron microscopy of *Hy-Tissue Nanofat* product after centrifugation. The square (in Fig. 1D, left) indicates the location of the higher magnification (Fig. 1D, right); the elastic fiber, the connective tissue lamina, and the single collagen fiber are shown with a dotted arrow, an asterisk, and an arrow, respectively [scale bar: (left) 50 µm, (right) 5 µm].

and $4.13 \times 10^5 \pm 1.15 \times 10^4$, respectively. Considering the enzymatic treatment as the gold standard protocol (cell yield 100%), the cellular yield for N-ASC resulted in 9.02% ± 3.18%, which increased to 28.98% ± 9.44% after the enzymatic digestion of the emulsion (N-ED-ASC), as reported in the table in Fig. 3A.

Cells were seeded in T-flasks until confluence to analyze the ASC adhesion and proliferation capacity (Fig. 3B, left). The results show that ED-ASC required less time to reach confluence (4.80 ± 2.28 days) than N-ASC (10.8 ± 2.59 days). This finding reflects the higher frequency of adherent cell content obtained with the enzymatic digestion of the fat. On the contrary, no significant statistical differences were shown between ED-ASC and N-ED-ASC (7.60 ± 3.29 days). Proliferation capacity results were confirmed with a PDT (Fig. 3B, right). PDT reveals that the replication rate of ED-ASC and N-ED-ASC was comparable (52.84 ± 6.40 and 57.06 ± 25.41 h, respectively), while cells obtained from N-ASC required more time to duplicate their number (81.85 ± 18.87 h). No statistical differences were found between N-ASC and N-ED-ASC, and N-ED-ASC and ED-ASC.

Fig. 3C shows a representative image of N-ASC, N-ED-ASC, and ED-ASC morphology 3 days after extraction (first culture media change). *Hy-Tissue Nanofat* treatment did not affect the cell morphology compared with cells obtained from enzymatic digestion, exhibiting a homogeneous fibroblast-like morphology. Moreover, cellular membranes and nuclei were well preserved, indicating no sign of cell suffering.

CFU-F assays were performed to assess the ability of the evaluated methods to grow as colonies. Fig. 4A shows a representative micrograph of CFU-F detected by toluidine blue staining after 14 days of seeding. On day 14, the morphology of CFU-F appeared comparable between the three treatments. The CFU-F yield of N-ASC was 61.29 ± 45.10

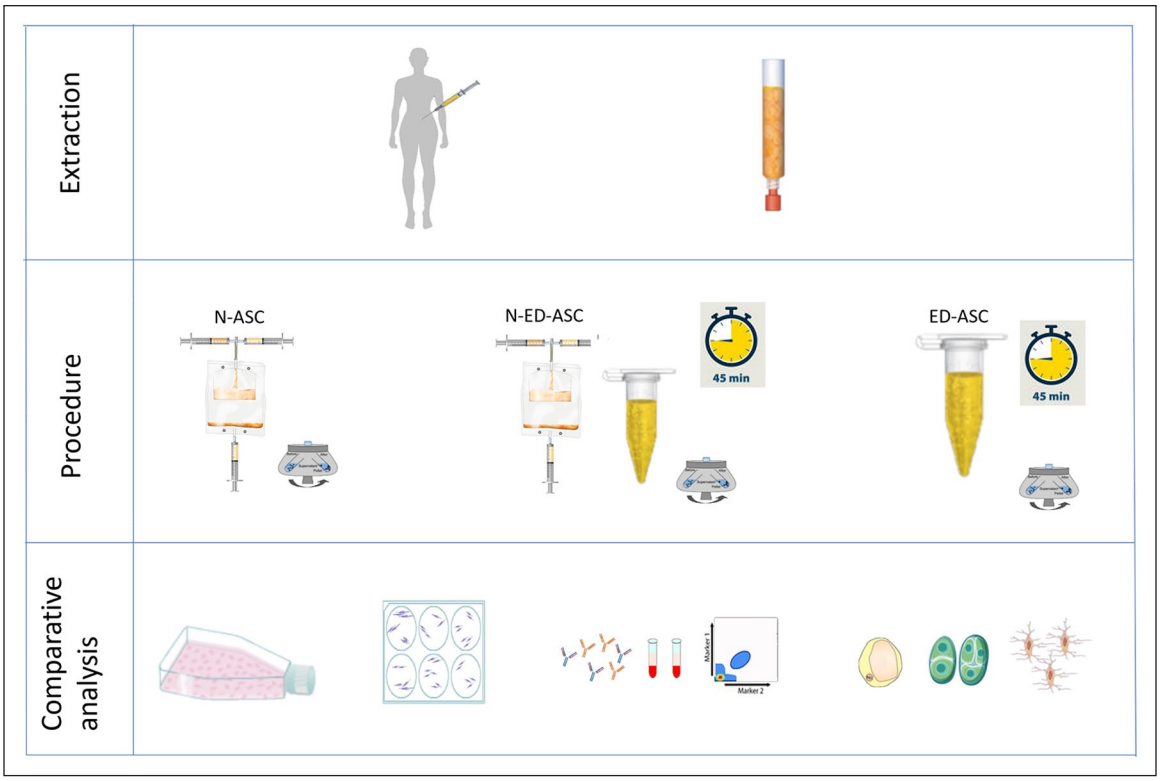

Figure 2. Experimental methodology. The fat samples were each divided into three portions to be processed in N-ASC, N-ED-ASC and ED-ASC and evaluated for cell proliferation capacity, CFU-F assay, immunophenotyping and differentiation potential. N-ASC: nanofat-derived adipose-derived stem cell; N-ED-ASC: enzymatic digestion of nanofat adipose-derived stem cell; ED-ASC: collagenase-derived adipose-derived stem cell; CFU-F: colony-forming unit-fibroblast.

CFU-F/ml FAT, while the CFU-F yield of N-ED-ASC increased over 11 times (702.29 ± 368.40 CFU/mL FAT; Fig. 4B). Furthermore, the relative proportion of CFU-F in the N-ED-ASC (0.54% ± 0.09%) increases significantly after the enzyme digestion of the emulsion compared with N-ASC (0.18% ± 0.05%; Fig. 4C). CFU-F obtained with ED-ASC was 29 and 3 times more (1,830.59 ± 1,190.82 CFU-F/mL FAT) compared with N-ASC and N-ASC-ED, respectively (Fig. 4B), with a relative proportion of CFU-F of 2.54% ± 0.69 % (Fig. 4C).

Immunophenotyping

To characterize N-ASC immunophenotypically, a cytofluorimetric analysis was performed immediately after the treatments (at cellular passage 0, P0) and after *in vitro* cellular expansion (cellular passage 2, P2). Specific single antigens (such as CD34, CD45, CD105, CD29, and CD73) were analyzed on the previously selected cells. The proportion of CD34 cells in N-ASC was 3.37% ± 1.67% (Fig. 5A), not thus far from the percentage of CD34 expression obtained in N-ED-ASC and ED-ASC (7.99% ± 4.6% and 4.91% ± 2.5 %, respectively). The hematopoietic surface marker CD45 resulted in less expressed cells (1.27% ± 0.45%, 1.35% ± 0.71%, and 1.53% ± 0.40% for N-ASC, N-ED-ASC, and ED-ASC, respectively), as reported in Fig. 5B. Moreover, the frequency of CD105-, CD29-, and CD73-positive cells (mesenchymal stem cell marker) was evaluated. In N-ASC, the percentage of antibody expression was 15.9% ± 8.86%, 3.59% ± 2.00%, and 1.79 ± 0.23 % for CD105, CD29, and CD73, respectively (Fig. 5A), comparable with the results obtained for the same antibody in N-ED-ASC and ED-ASC (Fig. 5B). Finally, cultured cells (P2) were also analyzed to confirm the phenotype preservation over time (Fig. 5C). The immunophenotypic analysis after the cellular expansion showed that the surface marker expression profiles of N-ASC, N-ED-ASC and ED-ASC were comparable, revealing a low expression for CD45 and CD34 and a high expression for mesenchymal stem cell–associated markers such as CD105, CD73, and CD29 (Fig. 5C).

Analysis of Multipotency

The multilineage differentiation ability of N-ASC was determined by analyzing qualitatively and semi-quantitatively the ability of adherent cells to differentiate toward adipocytes, chondrocytes, and osteocytes. The differentiation assay was conducted for 4 and 9 days of evaluation after the induction with a selective medium containing lineage-specific induction factors for the lineages mentioned above.

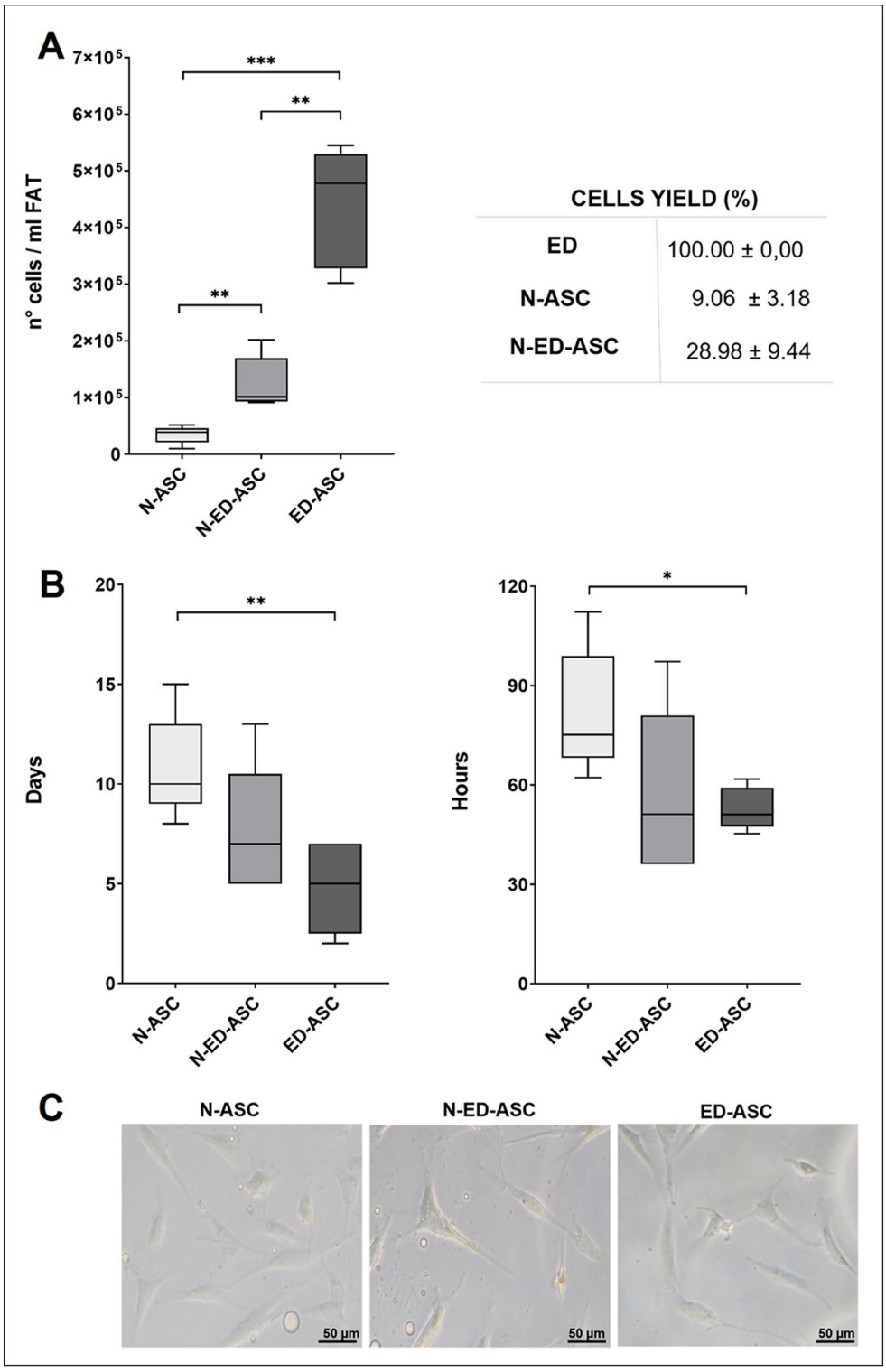

Figure 3. Cellular yield and proliferation capacity obtained with the three evaluated procedures of eight adipose tissue samples. (A) Nucleated cells obtained after the three evaluated treatments. Cell yield (no. of cell/ml FAT) was evaluated considering the enzymatic digestion as 100%. (B, left) Proliferation capacity of N-ASC, N-ED-ASC, and ED-ASC in T25 flasks. The days required for the adherent cells to reach confluence (passage 1) were counted. (B, right) The PDT of N-ASC, N-ED-ASC and ED-ASC was analyzed to evaluate the growth rate of adherent cells. No statistically significant differences were found between N-ASC and N-ED-ASC, and N-ED-ASC and ED-ASC. (C) Microscopic images of adherent cells 3 days after the extraction. All the results are shown as mean ± SD represented by error bars. Box and whisker plots represent the median. Significant statistical differences are indicated (*$P < 0.05$, **$0.005 < P < 0.001$, or ***$P < 0.001$). N-ASC: nanofat-derived adipose-derived stem cell; N-ED-ASC: enzymatic digestion of nanofat adipose-derived stem cell; ED-ASC: collagenase-derived adipose-derived stem cell; PDT: population doubling time assay.

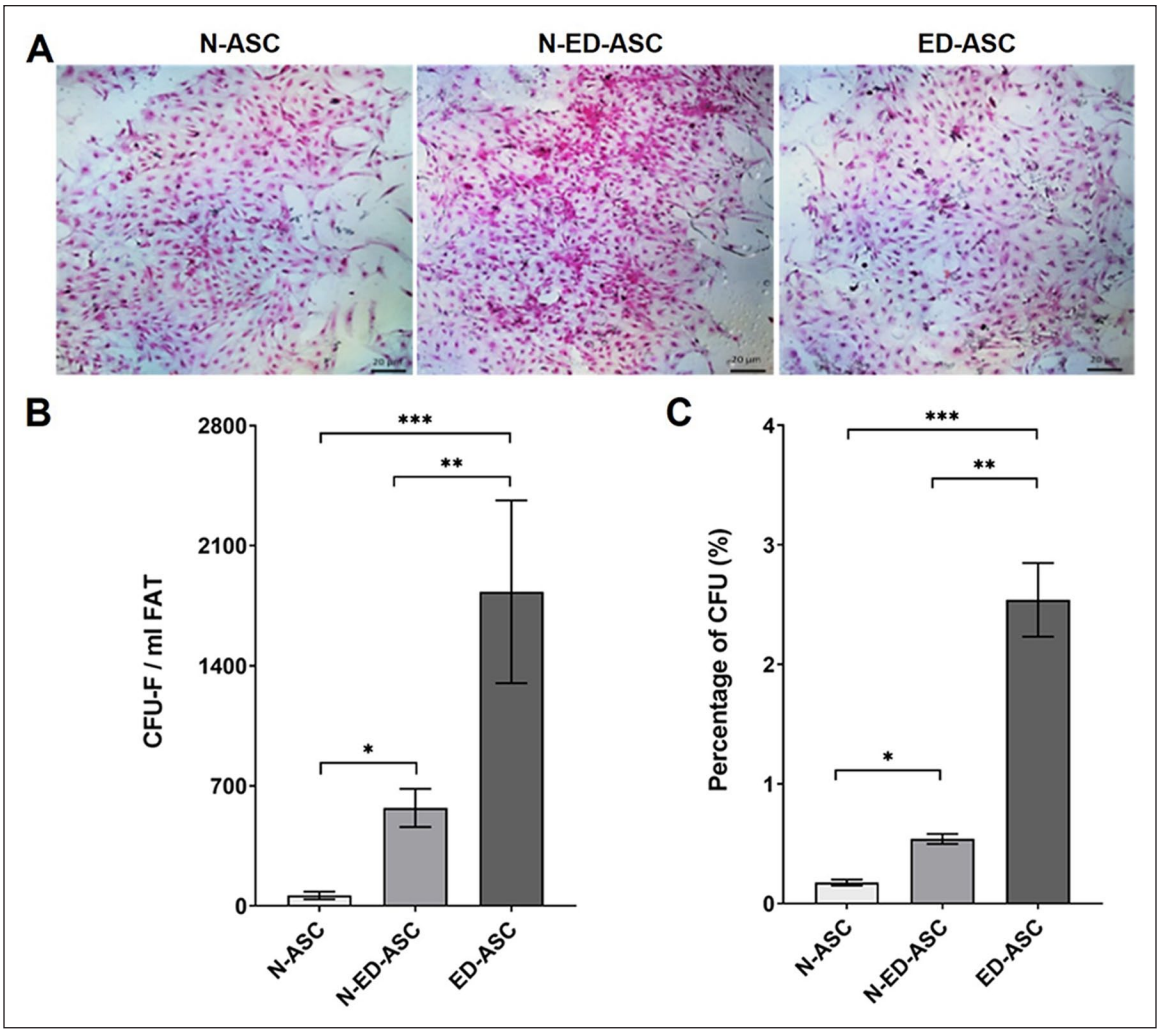

Figure 4. Clonogenic potential of Hy-Tissue Nanofat product ($n = 8$). (A) Representative light microscope of CFU-F assay stained with toluidine blue (scale bar, 20 µm). (B) CFU-F yields of N-ASC, N-ED-ASC, and ED-ASC. (C) Percentage of CFU-F of N-ASC, N-ED-ASC, and ED-ASC. All the results are shown as mean ± SD represented by error bars. Significant statistical differences are indicated (*$P <$ 0.05, **0.005 $< P <$ 0.001, or ***$P <$0.001). CFU-F: colony-forming unit-fibroblast; N-ASC: nanofat-derived adipose-derived stem cell; N-ED-ASC: enzymatic digestion of nanofat adipose-derived stem cell; ED-ASC: collagenase-derived adipose-derived stem cell.

Induced N-ASCs were stained with Oil-Red-Oil, Alizarin red, and Alcian blue to visualize the adipogenic, osteogenic, and chondrogenic differentiation, respectively, and the results were compared with ED-ASC and N-ED-ASC. Fig. 6A, B shows that N-ASCs were clearly differentiated into three mesodermal lineages on days 4 and 9. Applying the Oil-Red-Oil solution, red spots revealed the generation of lipid droplets on day 4, which increased in size due to the fusion of smaller lipid droplets during adipogenesis differentiation until day 9. Mature adipocytes are characterized by one lipid droplet of a size more significant than the cell nucleus that is formed by the fusion of small droplets[43]. In the case of osteogenic differentiation, Alizarin red staining shows the formation of *in vitro* calcification 4 days after medium induction with an intensification of the calcium deposits on day 9 of the study.

Similarly, the chondrogenic differentiation assay revealed that the generation of a cartilage-like matrix started from the fourth day upon the specific culture media induction. On day 9, a well-organized cartilage-like matrix rich in collagen III and sulfated proteoglycans was detectable, as shown with Alcian blue staining (Fig. 6A, B). Similarly, the multipotency assay was performed on N-ED-ASC and ED-ASC, showing positive staining compared with non-induced cells (CTR). For N-ED-ASC, the assay reveals that multilineage differentiation started on day 4, while ED-ASC differentiation started 9 days after the specific medium induction, suggesting a slower differentiation capacity than N-ASC for both methodologies. Fig. 6C shows the semi-quantitative analysis of the number of lipid droplets for the adipogenic differentiation, the calcified area for the osteogenic differentiation, and the cartilage-like matrix area for the chondrogenic

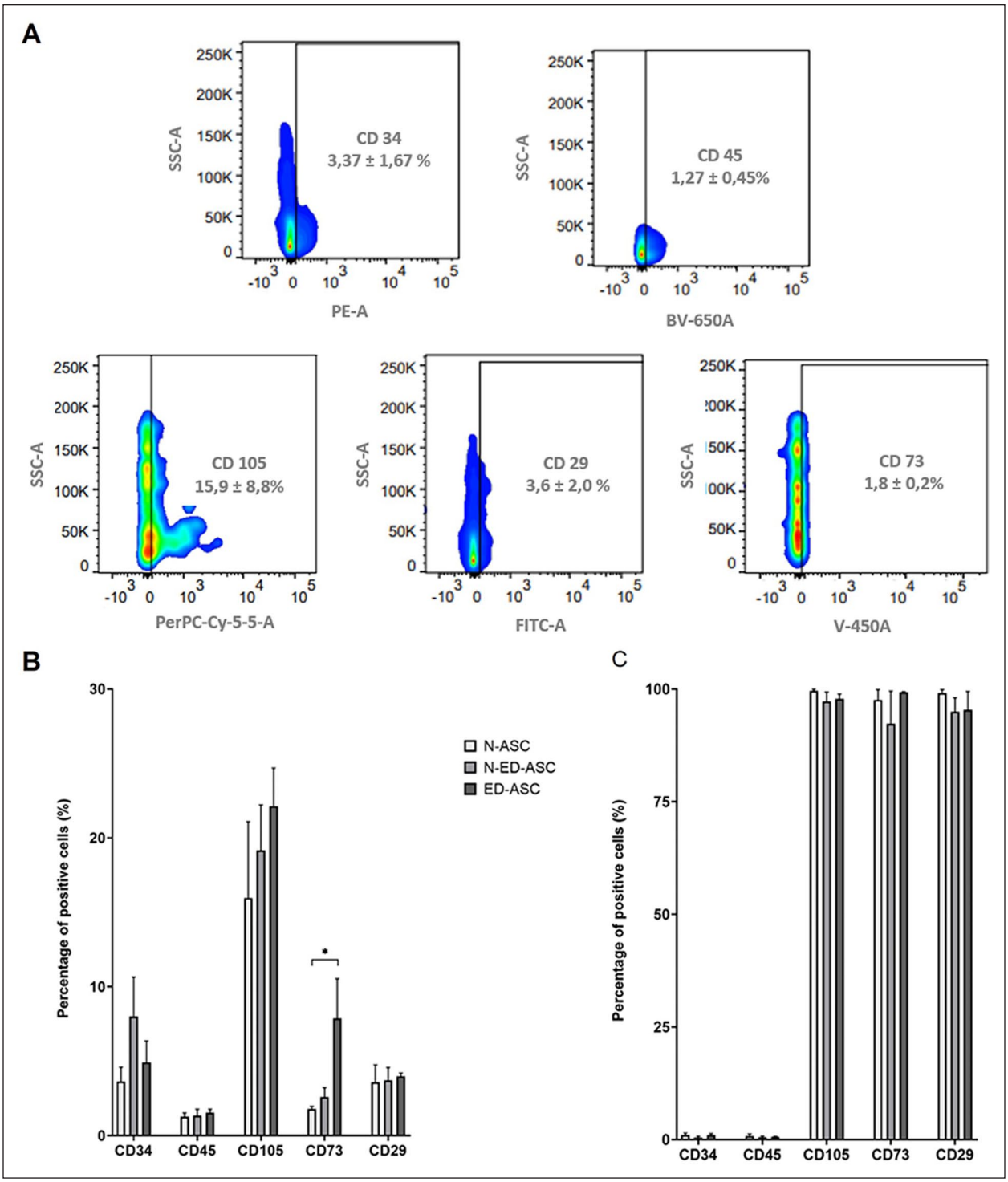

Figure 5. Surface markers expression was detected by flow cytometric analysis of N-ASC ($n = 8$). The percentage of positive cells for each marker was calculated after subtracting the non-specific fluorescence obtained with the control (unmarked). (A) Representative set of flow cytometry analysis for CD34, CD45, CD105, CD29, and CD73 markers performed on N-ASC. Percentage of positive cells to CD markers was indicated as an average of the samples; (B) percentage of positive cells to CD markers (as an average of the samples) in N-ASC compared with N-ED-ASC and ED-ASC; (C) percentage of positive cells to CD markers after *in vitro* cell expansion in N-ASC, N-ED-ASC, and ED-ASC. Results are presented as mean ± SD portrayed with error bars. Significant statistical differences are indicated (*$P < 0.05$). N-ASC: nanofat-derived adipose-derived stem cell; N-ED-ASC: enzymatic digestion of nanofat adipose-derived stem cell; ED-ASC: collagenase-derived adipose-derived stem cell.

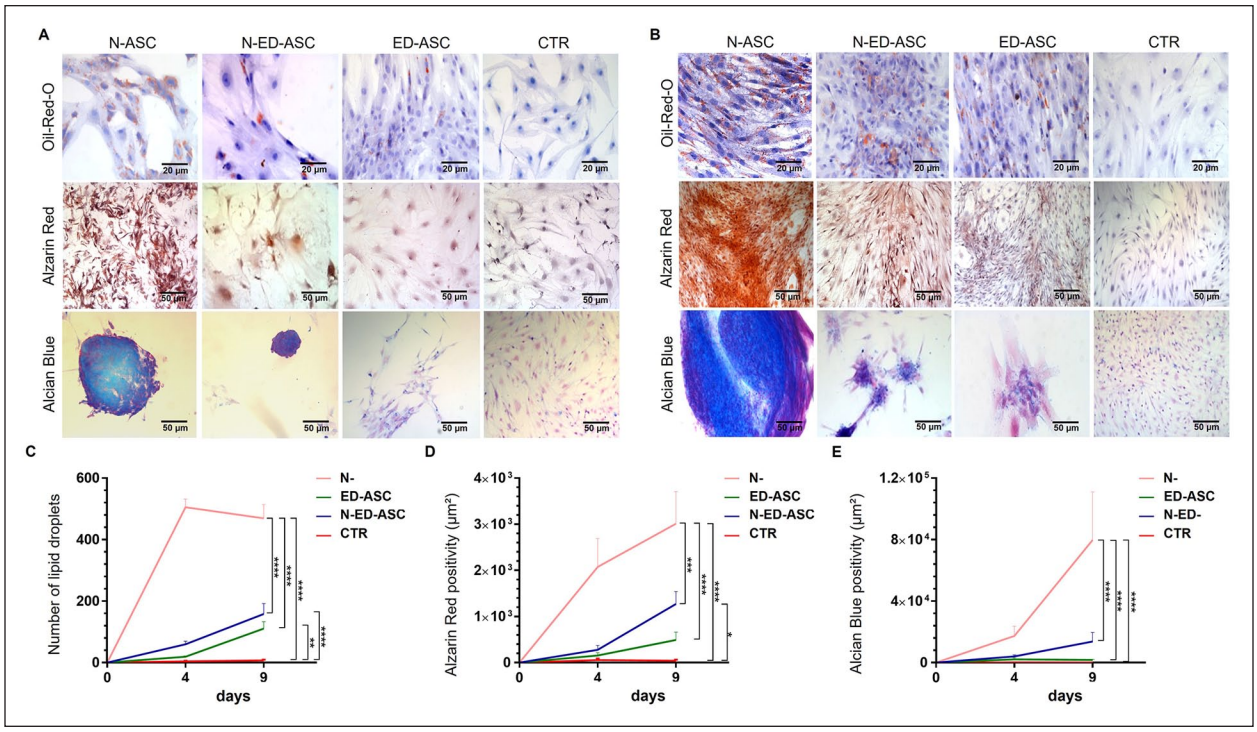

Figure 6. Multilineage differentiation assay ($n = 8$). (A) Optical microscopy images of induced N-ASC, N-ED-ASC, and ED-ASC and non-induced (CTR) cells with differentiation medium at day 4 (Oil-Red O staining scale bar, 10 µm; Alzarin red staining scale bar, 20 µm; Alcian blue staining scale bar, 10 µm); (B) optical microscopy images of induced N-ASC, N-ED-ASC, and ED-ASC and non-induced (CTR) cells with differentiation medium at day 9 (Oil-Red O staining scale bar 10 µm; Alzarin red staining scale bar 20 µm; Alcian blue staining scale bar, 10 µm). Red spots indicate the accumulation of neutral lipid vacuoles stained with Oil-Red-Oil; Alzarin red staining reveals in red the extracellular matrix calcification; deposition of sulfated proteoglycan-rich matrix is marked in blue with Alcian blue staining; (C) graph represents the mean amount of lipid droplets of the induced ASC. After 9 days of the induction, N-ASC shows higher lipid droplet formation than ED-ASC, N-ED-ASC, and CTR. (D) The graph showed the extracellular matrix calcification area measurement (µm²) of the induced ASC. After 9 days of treatment, N-ASC showed the highest calcium deposit formation. (E) The graph represents the area measurement of the generated cartilage-like matrix (µm²). On the ninth day, N-ASC showed the larger cartilage deposit formation. In graphics C, D and E, the pink line represents N-ASC, the green line ED-ASC, and the blue line N-ED-ASC. The data are presented as mean ± SD; significant statistical differences are indicated (*$P < 0.05$, **$0.05 < P < 0.001$, ***$P < 0.001$ or ****$P < 0.0001$). N-ASC: nanofat-derived adipose-derived stem cell; N-ED-ASC: enzymatic digestion of nanofat adipose-derived stem cell; ED-ASC: collagenase-derived adipose-derived stem cell; CTR: control.

differentiation. These results confirmed the previous optical analyses where the mean amount of lipid droplets for N-ASC after 4 days is higher than the one measured after 9 days of induction, indicating the fusion of small droplets to form larger ones that are characteristic of mature adipocytes. In addition, the number of lipid droplets after 9 days for N-ASC was 469.20 ± 44.35, which was higher than those found for ED-ASC (110.60 ± 22.81), N-ED-ASC (158.00 ± 34.10), and CTR (7.40 ± 2.29). In the same manner, the calcium deposition area was higher for N-ASC (3010.4 ± 699.4 µm²) compared with ED-ASC (493.2 ± 167.4 µm²), N-ED-ASC (1273.2 ± 268.7 µm²), and CTR (41.0 µm² ± 23.17 µm²) after 9 days of the osteogenic induction. Finally, the semi-quantification of the cartilage-like deposition area reveals a faster formation of a collagen matrix for the N-ASC (79716 ± 31360 µm²) in comparison with ED-ASC (1744 ± 372 µm²), N-ED-ASC (13740 ± 5944 µm²) and CTR (0 µm²) after 9 days of study.

To confirm the pluripotency of N-ASC, cells were then analyzed at flow cytometry to verify the presence of the MUSE cells, investigating the expression of SSEA-3 and CD-105 antibodies. Fig. 7A shows the percentage expression of the evaluated antibodies. N-ASC expressed 25.5% ± 6.5% of SSEA-3, while N-ED-ASC and ED-ASC expressed 3.12% ± 2.2% and 0.5% ± 0.2%, respectively. Finally, the immunofluorescence assay (Fig. 7B) confirmed the presence of MUSE cells in N-ASC, revealing positive cells for the expression of CD105 and SEEA3 simultaneously.

Discussion and Conclusion

Nanofat is a simple and well-described procedure that allows small volumes of adipose tissue injection. The product obtained is an emulsified fat, rich in viable cells avoiding expansion or enzymatic treatments. The emulsification procedure reduces the size of adipose fragments harvested by

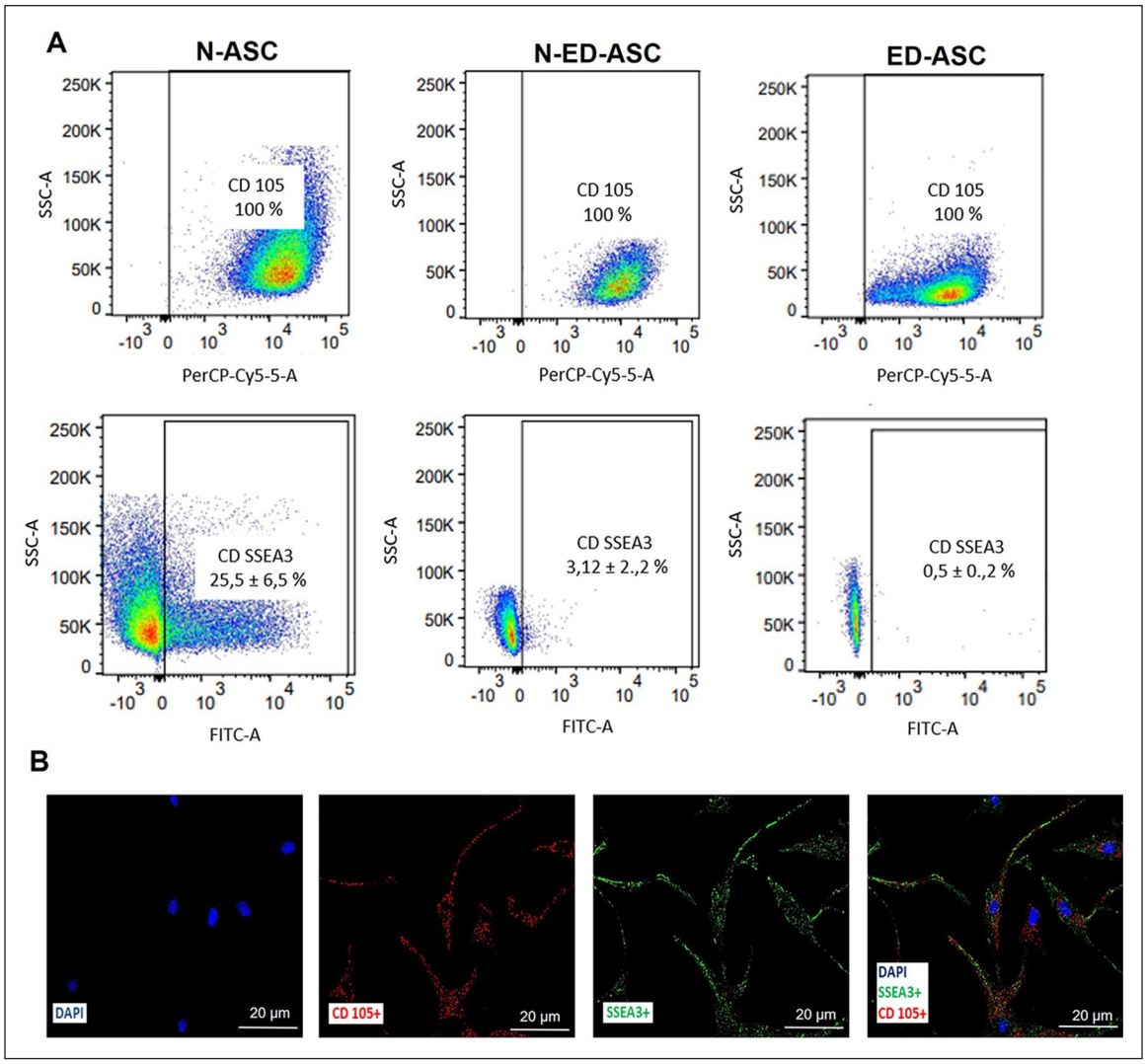

Figure 7. MUSE cell expression ($n = 8$). (A) Flow cytometry of N-ASC, N-ED-ASC, and ED-ASC to investigate the presence of MUSE cells. The percentage of positive cells to SEEA-3 and CD105 markers was indicated as an average of three samples, and the results are presented as mean ± SD. (B) Immunofluorescence microscopy of MUSE cells. MUSE cells in N-ASC were detected as positive cells for CD105 (left), SEEA3 (middle), and the simultaneous expression of CD105-SEEA3 (right). N-ASC: nanofat-derived adipose-derived stem cell; N-ED-ASC: enzymatic digestion of nanofat adipose-derived stem cell; ED-ASC: collagenase-derived adipose-derived stem cell; MUSE: multilineage-differentiating stress-enduring.

liposuction by a delicate filtration, obtaining an immediately injectable product[44]. Thanks to its fluid consistency, surgeons have promoted nanofat for face treatment rejuvenation, volume restoration, wrinkles, hypertrophic and atrophic scars, and defect correction[9–12].

This micro-fragmentation is able to produce smaller adipose niches than traditional techniques of adipose tissue manipulation with enormous advantages, allowing ASCs to migrate easily from the adipose lobules. In addition, nanofat is a "gentle" fragmentation that enables the preservation of the regenerative components in connective niches increasing cellular vitality and migration rate and allowing a faster secretion of growth factors. This could be crucial in clinical practice because it provides more beneficial regenerative effects for patients as already seen with the use of skin micrografts for difficult-to-heal wound treatment[45].

Hy-Tissue Nanofat is a new, simple system that reduces the time of adipose tissue processing drastically and guarantees the survival of regenerative units. The device reduces the size of the fat microfragments obtained after emulsification by shuffling the lipoaspirates 30 times between two connected syringes and filtering the emulsified adipose tissue through a membrane of 120 µm. In this study, deep characterization of the product has been performed, and the abundance of regenerative cells has been described.

Morphological analysis of the emulsified fat shows the presence of lipid droplets of different dimensions, mainly ranging between 60 and 100 µm, making the product easy to

inject into the desired location with high precision and suitable for injection under challenging areas with thin skin. The liquid consistency of nanofat, which also contains several endogenous cytokines and growth factors that are beneficial for vascularization initiation, allows it to be easily injected or be loaded onto a scaffold for various applications throughout the body[1,46].

The microanatomy of emulsified fat is primarily comparable to that of native adipose tissue, with capillaries and microvessels organized and disseminated between adipocytes, and pericytes wrapped around endothelial cells. Consequently, if the therapeutic value of Hy-Tissue Nanofat is related to the extraction of the adipose-connective niche, those complexes (cells, extracellular matrix, and ASCs) might exercise their regenerative performance more indirectly, via growth factor secretion, than as progenitor cells.

In vitro results obtained with the *Hy-Tissue Nanofat* system have been compared with those obtained through enzymatic digestion (collagenase type I), considered the standard gold technique to purify mesenchymal stem cells[47,48], and with the enzymatic digestion of Nanofat-SVF. Specifically, this last procedure was performed to evaluate the total amount of regenerative units, in terms of mesenchymal stem cells, that contribute to tissue remodeling, rejuvenation, and regeneration, describing the real regenerative potential of the *Hy-Tissue Nanofat*-SVF. The results of cellular yield and CFU assay showed that N-ASCs were characterized by lower cellular yield and capacity to form colonies if compared with the classic enzymatic digestion used to collect regenerative units from adipose tissue. The cellular yield resulted in about 9% (N-ASC), which increased to 29% after the enzymatic digestion of the emulsion (N-ED-ASC), suggesting that the system was highly efficient in extracting nucleated cells. Indeed, the number of N-ED-ASC resulted in $1.20 \times 10^5 \pm 3.90 \times 10^4$cells employing 10 ml of lipoaspirate, not so far from the results obtained in Tonnard et al.[6] for 100 ml of lipoaspirates. Subsequently, duplication and clonogenic assays have been performed to characterize the regenerative units present in the *Hy-Tissue Nanofat*-SVF. The growth rate and the clonogenic capability of N-ASC resulted to be lower than ED-ASC, which agrees with cellular yield results. Mechanical emulsification represents the minimal manipulation required to consider the injection of Nanofat-SVF, an autologous fat implant. On the contrary, enzymatic digestion represents a stronger method to isolate regenerative units, higher in number but characterized by slower differentiation capability.

Previous studies established that $CD34^+$ cells represent a stem cell population with higher proliferative capacity. Immunophenotypic analysis of N-ASC reveals 3.37% ± 1.67% of $CD34^+$-expressing marker, which is in accordance with the literature[23]. Tonnard et al.[6] have reported 4.5%–6.5% of CD34+ cells in nanofat-SVF. Moreover, a non-statistically significant difference has been noted between the treatments. When cultured, cells acquired a strong mesenchymal stem cell phenotype, increasing the expression of specific surface markers (CD73, CD105, and CD 29) and confirming phenotype maintenance after four passages in culture.

N-ASCs have also been tested for the capacity to differentiate into three mesenchymal cell types: adipocytes, osteocytes, and chondrocytes. The differentiation ability was evaluated after 4 and 9 days from specific media induction. N-ASCs can efficiently differentiate starting from the fourth day, underling a higher differentiation potential comparable with cells enzymatically extracted. Usually, the uptake of lipid droplets, a marker of adipogenic differentiation, is detectable between 10 and 14 days after media stimulation[6,15,29,30], while the calcification and proteoglycan matrix formation are detectable after 21 days[15,29,30].

In addition, N-ASC was immunophenotypically analyzed for SEEA3 expression as a specific marker for a subpopulation of mesenchymal stem cells called MUSE cells[31–35,36]. These cells are composed of pluripotent mesenchymal stem cells, able to migrate in damaged areas, as described in different preclinical and clinical models[49–51]. The results showed that N-ASC expressed 25.5% ± 6.5% of SEEA3 marker, while ED-ASC expressed 0.5% ± 0.2%. This difference might be due to the mechanical manipulation of fat tissue since MUSE cells are mainly expressed after severe cellular stress conditions[29,34]. These cells differentiate in numerous tissues, not only of mesenchymal origin, in a short time and could support the results obtained with differentiation assay. The use of emulsion fat-enriched MUSE cells in regenerative medicine could represent a novel aspect, increasing the treatment efficacy and the recovery time, even if a deeper analysis to understand the mechanism that undergoes high differentiation potential and MUSE expression is necessary.

Mainly, it is known that tissue enzymatic disaggregation can cause alterations in gene expression[52] and exosome amount[53], and this research displays how much the emulsified adipose tissue seems to be enriched with growth factors that are necessary to promote the reparative actions in damaged tissues[54,55]. Taken together, our data reveal a greater regenerative and differentiation impact of the adipo-connective niches that emerge from this "gentle micro-fragmentation," which provides the basis on which to build an explanation of therapeutic superiority. These results indicate *Hy-Tissue Nanofat* as a rapid, standardized, and efficient system able to produce an emulsion fat rich in viable, proliferative, and multipotent ASCs, suggesting a potential use in regenerative medicine and tissue engineering when translated into clinical practice. The regenerative potential of nanofat product is a safer alternative treatment given its intrinsic immunomodulatory, antiapoptotic, angiogenic, and proliferative factors without administering whole cells. Nevertheless, further research is needed to understand the specific role of nanofat secretome in repairing damaged and diseased tissues.

Acknowledgments

The authors thank Centro Piattaforme Tecnologiche (CPT, University of Verona, Italy) for their technical contribution.

Author Contributions

Experimental planning: A.B. and G.C.; data curation: A.B and L.A.Q.S.; investigation, A.B., R.B., A.C., R.O, S.S., S.M; formal analysis, A.B., F.D.F.; visualization, A.B., L.A.Q.S., A.C, R.O; writing—original draft, A.B., G.C, L.A.Q.S; writing—review and editing, A.B., F.D.F., L.A.Q.S.; project administration, A.S., M.R.; supervision and resources, M.R., A.S. All the authors have made substantial intellectual contributions to the evolution of the concepts presented in the manuscript and approved the final version submitted. All authors have read and agreed to the published version of the manuscript.

Availability of Data and Materials

Not applicable.

Ethical Approval

This study was approved by our institutional review board.

Statement of Human and Animal Rights

This article does not contain any studies with human or animal subjects.

Statement of Informed Consent

There are no human subjects in this article and informed consent is not applicable.

Research Ethics and Patient Consent

The study respects all ethical requirements in its targets and methodologies. We strictly comply with extensively identified global codes of practice inclusive of the Nuremberg Code, the Helsinki settlement, and the conventions of the Council of Europe on human rights and biomedicine, with a specific interest in European law: 2001/eighty-three/ec, 86/609/eec and fp7 selection nr 1982/2006ec. Human organic samples are essential due to the fact we want to test human cells, which have unique, organic traits distinct from the ones of animals. The general goal of this undertaking is to reduce the range of animal experiments. Adult patients who are capable of supplying consent became protected. All patients, which might be the topics of our observations, donated their consensus to scientific remedies and an eBook of their hospital situation and images. We have acquired written, informed consent from all patients. This was authorized by means of our inner moral committee (CARU—University of Verona), with authorization provided through human research committee number 2/2019.

Declaration of Conflicting Interests

The author(s) declared no potential conflicts of interest with respect to the research, authorship, and/or publication of this article.

Funding

The author(s) disclosed receipt of the following financial support for the research, authorship, and/or publication of this article: This support for publication of this article by Fidia Farmaceutici spa (Via Ponte della Fabbrica, 3/A - 35031 Abano Terme (PD)).

ORCID iDs

Lindsey Alejandra Quintero Sierra https://orcid.org/0000-0001-7336-0099

Francesco De Francesco https://orcid.org/0000-0003-2977-7828

References

1. Grünherz L, Sanchez-Macedo N, Frueh FS, McLuckie M, Lindenblatt N. Nanofat applications: from clinical esthetics to regenerative research. Curr Opin Biomed Eng. 2019;10:174–80.
2. Eto H, Kato H, Suga H, Aoi N, Doi K, Kuno S, Yoshimura K. The fate of adipocytes after nonvascularized fat grafting. Plast Reconstr Surg. 2012;129:1081–92.
3. Gir P, Brown SA, Oni G, Kashefi N, Mojallal A, Rohrich RJ. Fat grafting. Plast Reconstr Surg. 2012;130:249–58.
4. Kato H, Mineda K, Eto H, Doi K, Kuno S, Kinoshita K, Kanayama K, Yoshimura K. Degeneration, regeneration, and cicatrization after fat grafting: dynamic total tissue remodeling during the first 3 months. Plast Reconstr Surg. 2014;133(3):303e–313e.
5. Coleman SR, Lam S, Cohen SR, Bohluli B, Nahai F. Fat grafting. Atlas Oral Maxillofac Surg Clin. 2018;26:81–84.
6. Tonnard P, Verpaele A, Peeters G, Hamdi M, Cornelissen M, Declercq H. Nanofat grafting. Plast Reconstr Surg. 2013;132:1017–26.
7. Lindenblatt N, van Hulle A, Verpaele AM, Tonnard PL. The role of microfat grafting in facial contouring. Aesthetic Surg J. 2015;35:763–71.
8. Mesguich Batel F, Bertrand B, Magalon J, François P, Velier M, Veran J, Mallet S, Jouve E, Sabatier F, Casanova D. Traitement des ridules de la lèvre supérieure par graisse émulsifiée ou « Nanofat » : étude biologique et clinique à propos de 4 cas. Ann Chir Plast Esthétique. 2018;63:31–40.
9. Gu Z, Li Y, Li H. Use of condensed nanofat combined with fat grafts to treat atrophic scars. JAMA Facial Plast Surg. 2018;20:128–35.
10. Uyulmaz S, Sanchez Macedo N, Rezaeian F, Giovanoli P, Lindenblatt N. Nanofat grafting for scar treatment and skin quality improvement. Aesthetic Surg J. 2018;38:421–28.
11. Bhooshan LS, Devi MG, Aniraj R, Binod P, Lekshmi M. Autologous emulsified fat injection for rejuvenation of scars: a prospective observational study. Indian J Plast Surg. 2018;51(1):77–83.
12. Martin A, Maladry D, Esmaeli A, Gaucher S, Philippe HJ. Fat grafting of hairy areas of head and neck—comparison between lipofilling and nanofat grafting procedures in a cadaveric study. J Stomatol Oral Maxillofac Surg. 2018;119(4):274–78.
13. Gimble JM, Bunnell BA, Guilak F. Human adipose-derived cells: an update on the transition to clinical translation. Regen Med. 2012;7(2):225–35.
14. Bora P, Majumdar AS. Adipose tissue-derived stromal vascular fraction in regenerative medicine: a brief review on biology and translation. Stem Cell Res Ther. 2017;8:145.
15. Wei H, Gu S-X, Liang Y-D, Liang Z-J, Chen H, Zhu M-G, Xu F-T, He N, Wei X-J, Li H-M. Nanofat-derived stem cells with platelet-rich fibrin improve facial contour remodeling and skin rejuvenation after autologous structural fat transplantation. Oncotarget. 2017;8:68542–56.

16. Lo Furno D, Tamburino S, Mannino G, Gili E, Lombardo G, Tarico MS, Vancheri C, Giuffrida R, Perrotta RE. Nanofat 2.0: experimental evidence for a fat grafting rich in mesenchymal stem cells. Physiol Res. 2017;66::663–71.
17. Kachgal S, Putnam AJ. Mesenchymal stem cells from adipose and bone marrow promote angiogenesis via distinct cytokine and protease expression mechanisms. Angiogenesis. 2011;14(1):47–59.
18. Clevers H, Loh KM, Nusse R. An integral program for tissue renewal and regeneration: Wnt signaling and stem cell control. Science. 2014;346:1248012.
19. Rigotti G, Marchi A, Sbarbati A. Adipose-derived mesenchymal stem cells: past, present, and future. Aesthetic Plast Surg. 2009;33(3):271–73.
20. Dai R, Wang Z, Samanipour R, Koo KI, Kim K. Adipose-derived stem cells for tissue engineering and regenerative medicine applications. Stem Cells Int. 2016;2016:6737345.
21. Shang Q, Bai Y, Wang G, Song Q, Guo C, Zhang L, Wang Q. Delivery of adipose-derived stem cells attenuates adipose tissue inflammation and insulin resistance in obese mice through remodeling macrophage phenotypes. Stem Cells Dev. 2015;24:2052–64.
22. Prasai A, El Ayadi A, Mifflin RC, Wetzel MD, Andersen CR, Redl H, Herndon DN, Finnerty CC. Characterization of adipose-derived stem cells following burn injury. Stem Cell Rev Rep. 2017;13(6):781–92.
23. Kotani T, Masutani R, Suzuka T, Oda K, Makino S, Ii M. Anti-inflammatory and anti-fibrotic effects of intravenous adipose-derived stem cell transplantation in a mouse model of bleomycin-induced interstitial pneumonia. Sci Rep. 2017;7:14608.
24. Kalinina N, Kharlampieva D, Loguinova M, Butenko I, Pobeguts O, Efimenko A, Ageeva L, Sharonov G, Ischenko D, Alekseev D, Grigorieva O. Characterization of secretomes provides evidence for adipose-derived mesenchymal stromal cells subtypes. Stem Cell Res Ther. 2015;6:221.
25. Charles-de-Sá L, Gontijo-de-Amorim NF, Maeda Takiya C, Borojevic R, Benati D, Bernardi P, Sbarbati A, Rigotti G. Antiaging treatment of the facial skin by fat graft and adipose-derived stem cells. Plast Reconstr Surg. 2015;135(4): 999–1009.
26. De Francesco F, Tirino V, Desiderio V, Ferraro G, D'Andrea F, Giuliano M, Libondi G, Pirozzi G, De Rosa A, Papaccio G. Human CD34+/CD90+ ASCs are capable of growing as sphere clusters, producing high levels of VEGF and forming capillaries. Plos One. 2009;4:e6537.
27. Kober J, Gugerell A, Schmid M, Zeyda M, Buchberger E, Nickl S, Hacker S, Ankersmit HJ, Keck M. Healing effect of conditioned media obtained from adipose tissue on human skin cells: a comparative in vitro study. Ann Plast Surg. 2016;77:156–63.
28. Paliwal S, Chaudhuri R, Agrawal A, Mohanty S. Regenerative abilities of mesenchymal stem cells through mitochondrial transfer. J Biomed Sci. 2018;25:31.
29. Dai Prè E, Busato A, Mannucci S, Vurro F, De Francesco F, Riccio V, Solito S, Biswas R, Bernardi P, Riccio M, Sbarbati A. In vitro characterization of adipose stem cells non-enzymatically extracted from the thigh and abdomen. Int J Mol Sci. 2020;21:3081.
30. Busato A, De Francesco F, Biswas R, Mannucci S, Conti G, Fracasso G, Conti A, Riccio V, Riccio M, Sbarbati A. Simple and rapid non-enzymatic procedure allows the isolation of structurally preserved connective tissue micro-fragments enriched with SVF. Cells. 2020;10:36.
31. Kushida Y, Wakao S, Dezawa M. Muse cells are endogenous reparative stem cells. Adv Exp Med Biol. 2018;1103:43–68.
32. Conti G, Zingaretti N, Amuso D, Dai Prè E, Brandi J, Cecconi D, Manfredi M, Marengo E, Boschi F, Riccio M, Amore R, et al. Proteomic and ultrastructural analysis of cellulite-new findings on an old topic. Int J Mol Sci. 2020;21:2077.
33. Conti G, Bertossi D, Dai Prè E, Cavallini C, Scupoli MT, Ricciardi G, Parnigotto P, Saban Y, Sbarbati A, Nocini PF. Regenerative potential of the Bichat fat pad determined by the quantification of multilineage differentiating stress enduring cells. Eur J Histochem. 2018;62:2900.
34. Fisch SC, Gimeno ML, Phan JD, Simerman AA, Dumesic DA, Perone MJ, Chazenbalk GD. Pluripotent nontumorigenic multilineage differentiating stress enduring cells (Muse cells): a seven-year retrospective. Stem Cell Res Ther. 2017;8:227.
35. Simerman AA, Phan JD, Dumesic DA, Chazenbalk GD. Muse cells: nontumorigenic pluripotent stem cells present in adult tissues—a paradigm shift in tissue regeneration and evolution. Stem Cells Int. 2016;2016:1463258.
36. Wakao S, Kitada M, Kuroda Y, Shigemoto T, Matsuse D, Akashi H, Tanimura Y, Tsuchiyama K, Kikuchi T, Goda M, Nakahata T, et al. Multilineage-differentiating stress-enduring (Muse) cells are a primary source of induced pluripotent stem cells in human fibroblasts. Proc Natl Acad Sci U S A. 2011;108:9875–80.
37. Ogura F, Wakao S, Kuroda Y, Tsuchiyama K, Bagheri M, Heneidi S, Chazenbalk G, Aiba S, Dezawa M. Human adipose tissue possesses a unique population of pluripotent stem cells with nontumorigenic and low telomerase activities: potential implications in regenerative medicine. Stem Cells Dev. 2014;23:717–28.
38. Simerman AA, Dumesic DA, Chazenbalk GD. Pluripotent muse cells derived from human adipose tissue: a new perspective on regenerative medicine and cell therapy. Clin Transl Med. 2014;3:12.
39. Liu Q, Zhang RZ, Li D, Cheng S, Yang YH, Tian T, Pan XR. Muse cells, a new type of pluripotent stem cell derived from human fibroblasts. Cell Reprogram. 2016;18(2):67–77.
40. Martinello T, Bronzini I, Maccatrozzo L, Iacopetti I, Sampaolesi M, Mascarello F, Patruno M. Cryopreservation does not affect the stem characteristics of multipotent cells isolated from equine peripheral blood. Tissue Eng Part C Methods. 2010;16(4):771–81.
41. Li Q, Xu R, Lei K, Yuan Q. Insights into skeletal stem cells. Bone Res. 2022;10:61.
42. Suo J, Zou S, Wang J, Han Y, Zhang L, Lv C, Jiang B, Ren Q, Chen L, Yang L, Ji P, Zheng X, Hu P, Zou W. The RNA-binding protein Musashi2 governs osteoblast-adipocyte lineage commitment by suppressing PPARγ signaling. Bone Res. 2022;10:1–12.
43. Weidlich D, Honecker J, Boehm C, Ruschke S, Junker D, Van AT, Makowski MR, Holzapfel C, Claussnitzer M, Hauner H, Karampinos DC. Lipid droplet–size mapping in human adipose tissue using a clinical 3T system. Magn Reson Med. 2021;86(3):1256–70.
44. Kamat P, Frueh FS, McLuckie M, Sanchez-Macedo N, Wolint P, Lindenblatt N, Plock JA, Calcagni M, Buschmann J.

Adipose tissue and the vascularization of biomaterials: stem cells, microvascular fragments and nanofat—a review. Cytotherapy. 2020;22(8):400–11.
45. Riccio M, Marchesini A, Zingaretti N, Carella S, Senesi L, Onesti MG, Parodi PC, Ribuffo D, Vaienti L, De Francesco F. A multicentre study: the use of micrografts in the reconstruction of full—thickness posttraumatic skin defects of the limbs—a whole innovative concept in regenerative surgery. Stem Cells Int. 2019;2019:5043518.
46. Weinzierl A, Harder Y, Schmauss D, Menger MD, Laschke MW. Boosting tissue vascularization: nanofat as a potential source of functional microvessel segments. Front Bioeng Biotechnol. 2022;10:820835.
47. Peroni D, Scambi I, Pasini A, Lisi V, Bifari F, Krampera M, Rigotti G, Sbarbati A, Galiè M. Stem molecular signature of adipose-derived stromal cells. Exp Cell Res. 2008;314:603–15.
48. Alstrup T, Eijken M, Bohn AB, Møller B, Damsgaard TE. Isolation of adipose tissue-derived stem cells: enzymatic digestion in combination with mechanical distortion to increase adipose tissue-derived stem cell yield from human aspirated fat. Curr Protoc Stem Cell Biol. 2019;48(1):e68.
49. Yamasaki T, Wakao S, Kawaji H, Koizumi S, Sameshima T, Dezawa M, Namba H. Genetically engineered multilineage-differentiating stress-enduring cells as cellular vehicles against malignant gliomas. Mol Ther—Oncolytics. 2017;6:45–56.
50. Yabuki H, Wakao S, Kushida Y, Dezawa M, Okada Y. Human multilineage-differentiating stress-enduring cells exert pleiotropic effects to ameliorate acute lung ischemia–reperfusion injury in a rat model. Cell Transplant. 2018;27(6):979–93.
51. Mahmoud EE, Kamei N, Shimizu R, Wakao S, Dezawa M, Adachi N, Ochi M. Therapeutic potential of multilineage-differentiating stress-enduring cells for osteochondral repair in a rat model. Stem Cells Int. 2017;2017:8154569.
52. van den Brink SC, Sage F, Vértesy Á, Spanjaard B, Peterson-Maduro J, Baron CS, Robin C, van Oudenaarden A. Single-cell sequencing reveals dissociation-induced gene expression in tissue subpopulations. Nat Methods. 2017;14:935–36.
53. Garcia-Contreras M, Ricordi C, Robbins PD, Oltra E. Exosomes in the pathogenesis, diagnosis and treatment of pancreatic diseases. Cellr4 Repair Replace Regen Reprogram. 2014;2(1):e807.
54. De Francesco F, Gravina P, Busato A, Farinelli L, Soranzo C, Vidal L, Zingaretti N, Zavan B, Sbarbati A, Riccio M, Gigante A. Stem cells in autologous microfragmented adipose tissue: current perspectives in osteoarthritis disease. Int J Mol Sci. 2021;22:10197.
55. Senesi L, De Francesco F, Farinelli L, Manzotti S, Gagliardi G, Papalia GF, Riccio M, Gigante A. Mechanical and enzymatic procedures to isolate the stromal vascular fraction from adipose tissue: preliminary results. Front Cell Dev Biol. 2019;7:88.